Journal of Materials Physics and Chemistry, 2026, Vol. 14, No. 1, 11-21
Available online at http://pubs.sciepub.com/jmpc/14/1/2
Published by Science and Education Publishing
DOI:10.12691/jmpc-14-1-2

Improvement of the Physicochemical Properties of Clays Modified By Ferrihydrite

Bi Gamy Arsène Tra[1,2,*], Drissa Bamba[2], Alfred Niamien Kouamé[1], Namory Méité[1], Mariame Coulibaly[2], Koffi Léon Konan[1], Samuel Oyetola[1]

[1]Laboratory of Constitution and Reaction of Matter (LCRM), UFR SSMT, Félix Houphouët-Boigny University, Abidjan, Ivory Coast
[2]Laboratory of Fundamental and Applied Physical Sciences (LSPFA), École Normale Supérieure (ENS), Abidjan, Ivory Coast
*Corresponding author: arsenetrabi86@gmail.com

Received May 18, 2026; Revised June 19, 2026; Accepted June 26, 2026

Abstract This study aims to evaluate the effects of a combined treatment involving calcination at 750 °C, acid activation, and ferrihydrite doping on the physicochemical, mineralogical, and morphological properties of three natural clays from Côte d'Ivoire (KR, KB, and BB). To this end, physicochemical characterizations were performed on the raw samples, after calcination, and after ferrihydrite modification, in order to assess the influence of these treatments on the properties of the materials. The results indicate that calcination induces the transformation of kaolinite into amorphous metakaolinite, thereby enhancing structural disorder and promoting the formation of new reactive sites. Acid activation leads to an increase in porosity through the partial dissolution of aluminous phases, while ferrihydrite doping enriches the materials with iron oxyhydroxides and increases the density of surface hydroxyl groups. These modifications resulted in a significant improvement in the textural properties of the clays, with specific surface areas reaching 87.32 $m^2\ g^{-1}$ and iodine numbers as high as 1373 mg g^{-1}. Overall, the ferrihydrite-modified samples, particularly KR-Fe and KB-Fe, exhibited the most pronounced improvements in their physicochemical and textural characteristics, highlighting the potential of this modification strategy for the future development of low-cost materials for water treatment applications.

Keywords: *Modified clays, Ferrihydrite, Physicochemical properties, Adsorption*

Cite This Article: Bi Gamy Arsène Tra, Drissa Bamba, Alfred Niamien Kouamé, Namory Méité[1], Mariame Coulibaly, Koffi Léon Konan, and Samuel Oyetola, "Improvement of the Physicochemical Properties of Clays Modified By Ferrihydrite." *Journal of Materials Physics and Chemistry*, vol. 14, no. 1 (2026): 11-21. doi: 10.12691/jmpc-14-1-2.

1. Introduction

In many rural areas of developing countries, surface water constitutes the primary source of domestic water supply. However, these resources are frequently contaminated by inorganic, organic, and microbial pollutants, compromising their potability. Conventional treatment technologies, often costly and complex, remain largely inaccessible to the affected populations. In this context, adsorption has emerged as a simple, effective, and economically viable approach for water purification. Several low-cost materials have already demonstrated their potential for adsorption applications, including natural clays, modified activated carbons, and various lignocellulosic residues [1,2,3,4,5,6,7]. Among these materials, clays are of particular interest in Côte d'Ivoire because of their abundance and favorable surface properties [3,5,8]. However, the use of fine fractions obtained through particle-size separation techniques is often limited by aggregation phenomena, slow settling rates, and poor operational stability, which restrict their practical application in rural settings [9,10]. To overcome these limitations, the present study proposes the use of crushed and sieved clays as supports for the immobilization of iron hydroxides, which are recognized for their high affinity toward various contaminants [11,12,13]. Furthermore, the properties of clays, particularly kaolinite-rich clays, can be significantly enhanced through thermal and chemical treatments. Calcination induces the transformation of kaolinite into amorphous metakaolinite with increased reactivity, whereas acid activation promotes an increase in specific surface area, porosity, and the number of reactive surface sites [11,12]. Therefore, this work aims to characterize thermally treated clays subsequently modified by the deposition of iron oxyhydroxide (FeOOH) in order to assess the effects of these modifications on their physicochemical, mineralogical, morphological, and textural properties, and to explore their potential suitability for future applications in water treatment.

2. Materials and Methods

2.1. Raw Materials

This study focused on three natural clay samples collected from different regions of Côte d'Ivoire. The sampling locations are presented in Figure 1. The ochre-yellow clay sample, designated BB, was collected in Bongouanou, located in the Moronou region in central-eastern Côte d'Ivoire. The two other samples, designated KB and KR, exhibiting brown and reddish colors, respectively, were collected in Katiola, in the Hambol region of northern Côte d'Ivoire. The samples were excavated using a hoe and immediately stored in 15 kg nylon bags without any prior treatment. Prior to characterization, the samples were air-dried under shade at ambient temperature for several days, manually crushed to remove aggregates, and homogenized. A portion of each sample was then finely ground using an agate mortar and sieved through a 63 µm mesh sieve to obtain a homogeneous powder suitable for subsequent analyses.

2.2. Heat Treatment

The raw clay samples were subjected to thermal treatment in a Thermo Scientific furnace (Model F48020-33). Approximately 50 g of each sample was calcined at 750°C for 3h [14]. This treatment was intended to induce dehydroxylation of the clay minerals, promote the transformation of kaolinite into amorphous metakaolinite, remove residual organic matter, and modify the reactivity of the material. After calcination, the samples were allowed to cool to room temperature in a desiccator before further use.

2.3. Ferrihydrite Deposition

The calcined clay samples were first subjected to acid activation. Briefly, 50 g of calcined clay was dispersed in 100mL of 5 $mol \cdot L^{-1}$ hydrochloric acid (HCl) in a borosilicate glass reactor. The suspension was heated at 90°C under continuous magnetic stirring for 3h. After cooling to room temperature, the mixture was vacuum-filtered, and the recovered solid phase was repeatedly washed with distilled water until the filtrate reached approximately neutral pH (pH ≈ 7). The acid-treated material was subsequently dried at 60°C for 24h. This pretreatment was performed to partially dissolve alumina-rich phases, increase porosity, and expose additional reactive surface sites, thereby facilitating the subsequent immobilization of ferrihydrite. Ferrihydrite deposition was then carried out according to the procedure described by Dehou et al. [12]. Briefly, 30 g of the acid-treated metakaolinite was introduced into a closed reactor containing 100 mL of an aqueous ferrous sulfate solution ($FeSO_4 \cdot 7H_2O$, 0.29 $mol \cdot L^{-1}$), prepared by dissolving 80 g of $FeSO_4 \cdot 7H_2O$ in 1 L of distilled water. The pH of the suspension was gradually adjusted to approximately 7 by the dropwise addition of a 1 $mol \cdot L^{-1}$ sodium hydroxide (NaOH) solution under continuous magnetic stirring to promote the in situ precipitation and deposition of ferrihydrite onto the clay surface and within its porous structure. The reaction mixture was maintained under continuous stirring for 24h at room temperature in a closed system to minimize evaporation and external contamination. The resulting suspension was then vacuum-filtered, and the recovered solid was thoroughly washed with distilled water until complete removal of residual sulfate ions. Finally, the ferrihydrite-modified material was dried at 60°C for 24h prior to characterization. The closed-reactor approach employed in this study has been reported to be simple, effective, and suitable for ferrihydrite immobilization while requiring only minimal laboratory equipment [12,15].

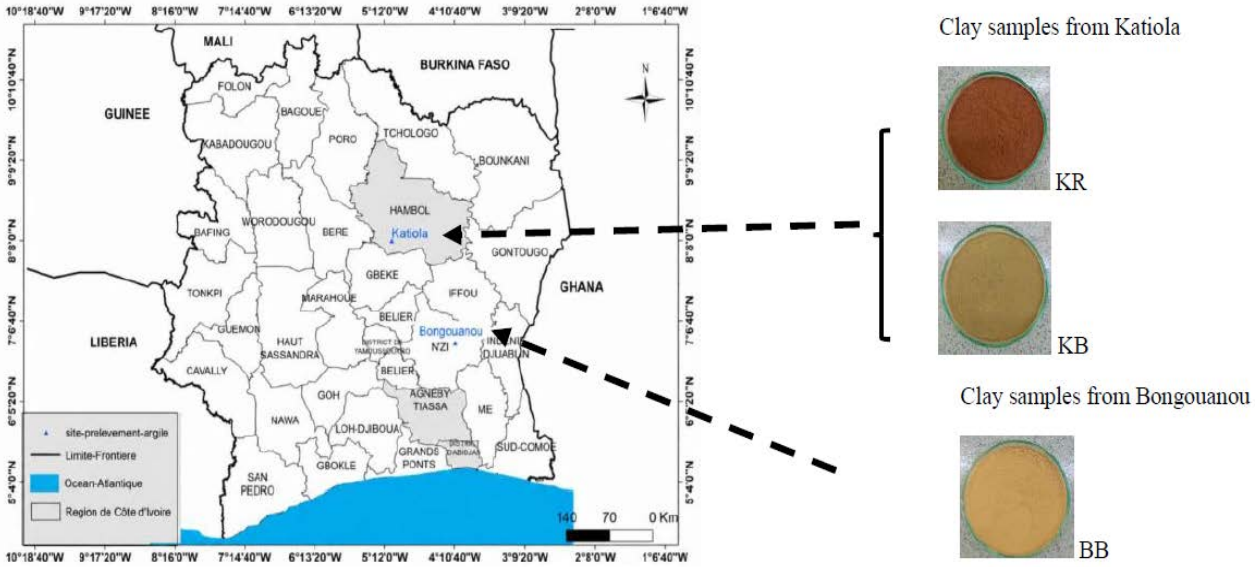

Figure 1. Location of clay sampling sites

2.4. Characterization Techniques

All experimental analyses were performed in triplicate to ensure the reproducibility of the results. The values reported in the tables correspond to the arithmetic means accompanied by their standard deviations. X-ray diffraction (XRD) analyses were carried out on raw clay samples sieved to a particle size of 63 µm. The samples were prepared according to the conventional powder diffraction method, which involves the analysis of finely ground dry powders without preferential crystallographic orientation. The measurements were performed using a Rigaku Miniflex powder diffractometer operating at 30 kV and 15 mA, with Cu Kα radiation (λ = 1.5418 Å). Diffractograms were recorded over a 2θ range of 5–60° at a scanning rate of 2° min^{-1}. Phase identification was achieved using Match software in combination with crystallographic databases. Fourier-transform infrared (FTIR) spectroscopy was employed to identify the functional groups and chemical bonds present in the clay samples through their characteristic vibrational bands. The infrared spectra were recorded using a computer-controlled Agilent Cary 630 FTIR spectrometer within the spectral range of 4000–400 cm^{-1}. The morphology and elemental composition of the samples were investigated using a Phenom ProX scanning electron microscope (SEM). The instrument was equipped with an OXFORD Instruments energy-dispersive X-ray spectroscopy (EDX) detector (Inca Dry-Cool microanalysis platform), which operates without the need for liquid nitrogen. The coupling of SEM and EDX techniques enabled the simultaneous observation of surface morphology and the determination of the elemental composition of selected areas of the samples. The chemical composition of the clay materials was determined by X-ray fluorescence (XRF), while the qualitative mineralogical composition was obtained from X-ray diffraction (XRD) analyses. The quantitative mineralogical composition was subsequently estimated by combining the XRF and XRD results using Equation (1) [16]:

$$T(a) = \sum M_i \times P_i(a) \quad (1)$$

T(a): percentage content (%) of oxide "a" in the sample; : percentage content (%) of mineral "i" in the sample; : proportion of oxide "a" in mineral "i" (this proportion is deduced from the ideal formula assigned to mineral "i"). The specific surface area of the samples was determined using the Brunauer–Emmett–Teller (BET) method. Prior to analysis, the samples were degassed under vacuum at 120 °C overnight to remove moisture and physically adsorbed species. Nitrogen adsorption–desorption measurements were subsequently carried out at 77 K using a Nova 4200e automated volumetric adsorption analyzer. The specific surface area was calculated from the adsorption isotherms according to the BET equation. The surface charge properties of the materials were evaluated through the determination of the point of zero charge (pH_pzc). This parameter corresponds to the pH at which the net surface charge of the solid is zero and plays a crucial role in controlling the interactions between the adsorbent surface and ionic species in aqueous media [5,6]. The iodine number was determined to assess the microporous characteristics of the materials, as this parameter reflects their affinity for small molecules and is commonly used as an indicator of micropore development. In addition, the methylene blue index was measured to evaluate the accessibility of larger molecules to the adsorbent surface and to provide information on the mesoporous characteristics of the materials [7].

3. Results and Discussion

3.1. Effects of Calcination and Ferrihydrite Deposition

The clay samples underwent various treatments designed to modify their physicochemical properties. Each treatment induced significant changes that varied according to the origin of the clay samples (Katiola or Bongouanou). After each treatment step, noticeable changes in color and texture were observed (Table 1). The raw clays, initially reddish (KR), yellowish-brown (KB), and light yellow (BB), turned grayish (KR-Cal, KB-Cal, and BB-Cal) after calcination at 750°C. These color changes suggest the occurrence of chemical and structural transformations [17], including the dehydroxylation of clay minerals and the partial disruption of the crystalline structure associated with the formation of metakaolinite [18]. Acid activation resulted in finer and lighter powders, which may be attributed to the partial dissolution of certain mineral phases and the removal of impurities from the clay matrix [19]. Following ferrihydrite deposition, the modified samples exhibited a reddish-brown coloration characteristic of iron oxyhydroxides, indicating the successful incorporation of iron-bearing phases onto the clay surface [19].

3.2. Physicochemical Modifications

The chemical composition of the clay samples, presented in Table 2, reveals the major oxides associated with the different mineral phases constituting the materials. The raw samples (KR, KB, and BB) exhibit noticeable chemical variability, reflecting differences in their geological origin and mineralogical composition. Silicon dioxide (SiO_2) contents range from 46.17 to 58.09 wt.%, indicating a significant contribution of siliceous phases, particularly quartz. Aluminum oxide (Al_2O_3) is also present in substantial amounts, with concentrations varying from 17.24 to 21.91 wt.%, suggesting the abundance of aluminosilicate minerals. In combination with the XRD results, these findings support the presence of clay minerals such as kaolinite and smectite in the investigated samples.

Table 1. Effects of Calcination and Ferrihydrite Deposition

Samples	Raw clays	Calcined clays	Leached clays	Ferrihydrite deposit
Katiola (KR)			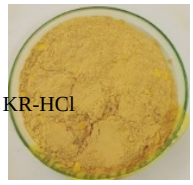	
Katiola (KB)	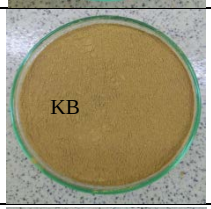		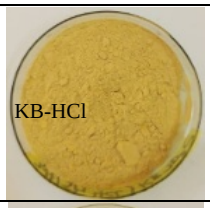	
Bongouanou (BB)			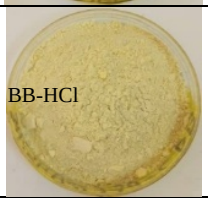	

Table 2. Chemical composition of the samples (% by mass)

Samples	SiO_2	Al_2O_3	Fe_2O_3	K_2O	Na_2O	MgO	MnO	TiO_2	CaO	PP_2O_5
BB	58.09	20.07	3.68	1.49	0.31	0.20	0.00	0.69	0.00	0.03
KB	49.92	17.24	9.26	1.67	1.21	1.90	0.06	0.76	1.23	0.07
KR	46.17	21.91	16.85	0.86	0.17	1.16	0.02	1.03	0.04	0.04
BB-Cal	60.01	27.42	5.32	1.62	0.16	0.28	0.00	1.2	0.02	0.06
KB-Cal	54.80	25.21	10.64	2.02	1.01	2.05	0.00	1.56	1.3	0.1
KR-Cal	48.5	28.67	17.02	1.07	0.09	1.25	0.00	2.03	0.06	0.08
BB-Fe	72.23	11.90	7.20	1.31	0.41	0.04	0.00	0.80	0.00	0.01
KB-Fe	68.71	8.3	12.05	1.52	1.58	0.89	0.02	0.98	0.73	0.05
KR-Fe	57.96	13.97	20.72	0.64	0.55	0.17	0.00	1.28	0.00	0.02

The concentrations of iron oxide (Fe_2O_3) vary considerably among the raw samples, ranging from 3.68 to 16.85 wt.%. This variability reflects differences in the abundance of iron-bearing phases, with iron occurring both as a structural constituent incorporated into the crystal lattice of phyllosilicates and as secondary minerals such as iron oxides and hydroxides, including goethite and hematite. These findings are consistent with those reported by Atsé et al. [20], Soro et al. [21], and Gauly et al. [22], who observed similar geochemical characteristics in clays collected from the Dabou, Bingerville, Adiaho, Zuenoula, Tanou-Sakassou, and Motiamo regions of Côte d'Ivoire. The P_2O_5 contents remain low (0.03–0.07 wt.%), suggesting a limited contribution of phosphate-bearing phases. Likewise, the relatively low concentrations of TiO_2 (0.69–1.03 wt.%) and CaO (0.04–1.23 wt.%) indicate a minor occurrence of titanium-bearing minerals (anatase and rutile) and carbonate phases (calcite and dolomite), respectively. Calcination at 750 °C (KR-Cal, KB-Cal, and BB-Cal) induced the dehydroxylation of phyllosilicates, particularly kaolinite, resulting in its transformation into amorphous metakaolinite. This transformation was accompanied by an apparent increase in Al_2O_3 and a slight enrichment in SiO_2 contents, which can be attributed to the elimination of volatile constituents and the concentration of the residual mineral phases. These observations are in agreement with the findings of Daou et al. [24], who reported that thermal treatment enhances the reactivity of clay materials through the development of structurally disordered sites. Acid activation using 5 $mol \cdot L^{-1}$ HCl at 90 °C promoted the selective dissolution of alumina-rich phases, as evidenced by the marked decrease in Al_2O_3 content, which reached 8.30 wt.% in the KB-Fe sample. Simultaneously, the relative proportion of SiO_2 increased, attaining 72.23 wt.% in BB-Fe, reflecting the enrichment of silica following the removal of phases more susceptible to acid attack. Subsequent ferrihydrite deposition led to a substantial increase in Fe_2O_3 contents, reaching 20.72 wt.% in KR-Fe. This increase provides indirect evidence of the successful incorporation of iron-bearing phases onto the clay matrix. The resulting modifications in chemical composition are consistent with the observations of Dehou [12], who highlighted the effectiveness of ferrihydrite deposition in altering the surface characteristics of clay materials intended for environmental applications.

3.3. X-ray Diffraction

X-ray diffraction (XRD) analysis was conducted on the raw clay samples (KR, KB, and BB) and their calcined counterparts (KR-Cal, KB-Cal, and BB-Cal) in order to investigate the mineralogical changes induced by calcination at 750°C. The diffractograms obtained enabled the identification and comparison of the crystalline phases present before and after heat treatment (Figure 2).

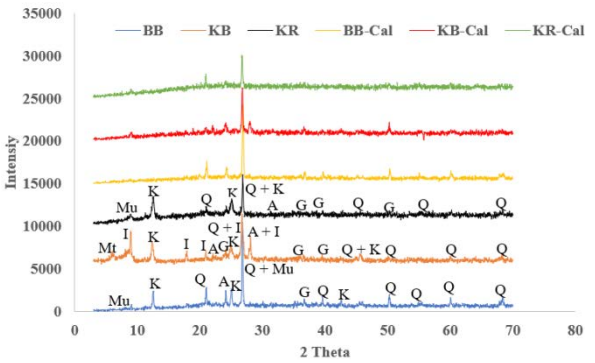

Figure 2. Diffractograms of raw and calcined clays at 750°C : Quartz (Q), Kaolinite (K), Albite (A), Muscovite (Mu), Goethite (G), Illite (I), and Montmorillonite (Mt)

The diffractograms of the raw clays reveal the predominant presence of quartz (Q) in all samples, as evidenced by its intense and well-defined diffraction peaks. Kaolinite (K) is also well represented, particularly by its characteristic reflections located at approximately 12.3° and 24.8° (2θ). Kaolinite is commonly reported in clay materials from Côte d'Ivoire [5,22,25,26,27]. In the KR and BB samples, muscovite (Mu) was identified, suggesting the presence of potassium-bearing phyllosilicates (Table 2). The KB sample contains, in addition to kaolinite, swelling clay minerals such as montmorillonite (Mt) and illite (I), indicating a more complex mineralogical composition and a probable mixed sedimentary origin. The occurrence of albite (A) in all raw samples suggests a common feldspathic contribution that has undergone limited weathering. Goethite (G) was also detected in the three raw clays, reflecting the ferruginous nature of these tropical weathering products [28]. Following calcination at 750°C, the diffractograms of the treated samples exhibited substantial mineralogical changes (Table 2). The characteristic peaks of kaolinite disappeared completely in KR-Cal, KB-Cal, and BB-Cal, indicating its transformation into amorphous metakaolinite through the dehydroxylation of the 1:1 aluminosilicate layers [29]. The montmorillonite reflections initially observed in KB were no longer detectable in KB-Cal, suggesting the collapse of the expandable structure under thermal treatment [30]. Illite, which exhibits greater thermal stability, showed a reduction in peak intensity in KB-Cal, indicating the onset of structural disorder [31]. Goethite, initially identified in the raw materials, disappeared after calcination, which may be attributed to its transformation into hematite at temperatures above 300–400°C [25,32]. Quartz remained the dominant and thermally stable phase in all calcined samples, with no significant changes in its diffraction pattern, confirming its resistance to thermal treatment at 750°C [33]. Similarly, albite preserved its crystalline structure, highlighting its stability under these conditions. Weak muscovite reflections persisted in some calcined samples, particularly KR-Cal and BB-Cal, although a progressive loss of crystallinity was observed. Overall, the transformation of phyllosilicate minerals into amorphous metakaolinite resulted in the development of a more disordered structure characterized by a reduced degree of crystallinity. Such structural modifications may influence the physicochemical and surface properties of the calcined materials and are consistent with the changes observed through complementary characterization techniques.

3.4. Mineralogical Composition

The theoretical results of the mineralogical composition of the clay samples are presented in Table 3.

Table 3. Semi-quantitative mineralogical composition of the samples

Samples	% Albite	% Goethite	% Muscovite	% Montmorillonite	% Kaolinite	% Illite	% Quartz
KR	1.44	18.75	7.28	-	47.63	-	19.73
KB	10.23	10.3	-	24.71	10.65	14.82	15.73
BB	2.62	4.09	12.62	-	37.20	-	33.28

Kaolinite is the dominant clay mineral in the KR and BB samples, accounting for 37.20–47.63 wt.%, whereas montmorillonite is the predominant clay phase in KB (24.71 wt.%). All the investigated clays contain albite and goethite, with contents ranging from 1.44 to 10.23 wt.% and from 4.09 to 18.75 wt.%, respectively. In contrast, montmorillonite and illite were identified exclusively in the KB sample, where they represent 24.71 wt.% and 14.82 wt.%, respectively. The relatively low goethite content observed in the BB sample (4.09 wt.%) may contribute to its lighter coloration [35]. The marked mineralogical differences among the studied clays are expected to influence their physicochemical properties. In particular, smectitic minerals such as montmorillonite are generally characterized by high specific surface areas and cation exchange capacities compared with kaolinite-rich clays [28,36,37]. Similarly, iron oxyhydroxides, including goethite, are known to possess reactive surface hydroxyl groups that can play an important role in interfacial processes occurring at the solid–solution interface [5]. For example, Aké et al. [38] reported that goethite-rich kaolinitic materials exhibited enhanced affinity toward phosphate species. Although such findings highlight the potential environmental relevance of these mineral phases, the present study focuses primarily on the characterization of the mineralogical modifications induced by the different treatments applied to the Ivorian clays.

3.5. FTIR Spectroscopic Analysis of Samples

FTIR analysis of the clay samples (Figures 3, 4, and 5) reveals significant structural modifications due to the various treatments applied. These analyses were performed in the wavenumber range of 600 to 4000 cm^{-1}.

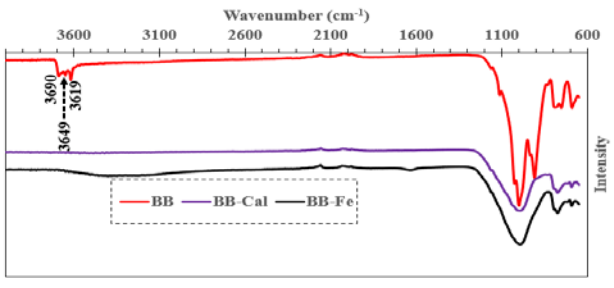

Figure 3. IR spectrum of BB, BB-Cal and BB-Fe samples

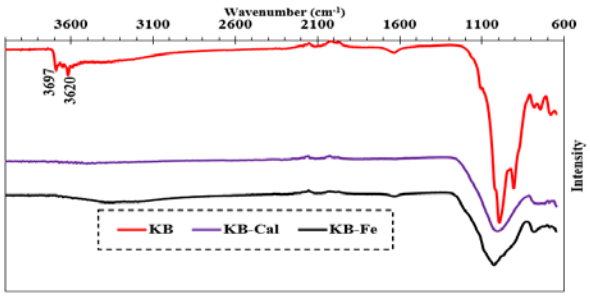

Figure 4. IR spectrum of KB, KB-Cal and KB-Fe samples

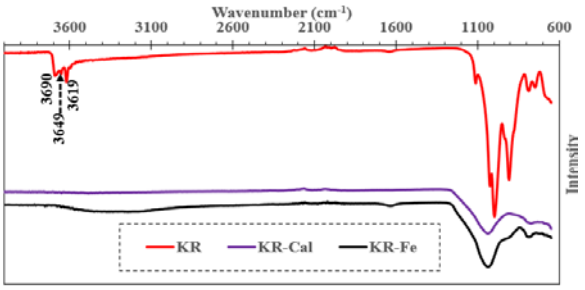

Figure 5. IR spectrum of KR, KR-Cal and KR-Fe samples

The Fourier-transform infrared (FTIR) spectra of the raw KR and BB samples exhibit similar spectral features. In the high-wavenumber region (3500–4000 cm^{-1}), three weak absorption bands are observed at 3690, 3649, and 3619 cm^{-1}, whereas the KB sample displays two bands centered at 3697 and 3620 cm^{-1}. These bands are characteristic of the stretching vibrations of structural hydroxyl groups (–OH) associated with kaolinite [39]. The bands located at 3690–3697 cm^{-1} and 3649 cm^{-1} are generally assigned to external hydroxyl groups situated on the surface or between adjacent layers, whereas the band observed at 3619–3620 cm^{-1}, common to all samples, corresponds to the stretching vibration of internal hydroxyl groups linked to the octahedral sheet of kaolinite [40]. In the intermediate spectral region (700–1800 cm^{-1}), several absorption bands related to the silicate framework, hydroxyl groups, and adsorbed water molecules are detected. The medium-intensity bands observed at 685, 735–754, and 783–791 cm^{-1}, characteristic of kaolinitic materials, are attributed to the deformation vibrations of hydroxyl groups and lattice translational modes [40]. The intense band centered around 908 cm^{-1}, present in all three raw samples, is assigned to the deformation vibration of Al–OH groups within the octahedral sheet of kaolinite [40]. In addition, the bands at 1622 cm^{-1} (KB) and 1632 cm^{-1} (KR and BB) are associated with the bending vibrations of hydroxyl groups from physically adsorbed water molecules [5]. Finally, the bands located between 989 and 1125 cm^{-1} (989, 998, 1007, 1021, 1025, 1106, and 1125 cm^{-1}) correspond to the stretching vibrations of Si–O bonds characteristic of aluminosilicate structures [40]. Thermal treatment of the samples (KR-Cal, KB-Cal, and BB-Cal) induced significant modifications in the FTIR spectra. In particular, attenuation and slight shifts of the Si–O and Si–O–Si bands were observed, indicating distortions within the tetrahedral framework and the progressive loss of structural order in the aluminosilicate matrix. The disappearance of the characteristic Al–OH bands associated with kaolinite in the calcined samples provides evidence for dehydroxylation and the breakdown of the octahedral layers, in agreement with the formation of amorphous metakaolinite reported in the literature [41,42,43]. The calcined samples were subsequently modified through hydrochloric acid treatment followed by ferrihydrite deposition, resulting in noticeable spectral changes in the KR-Fe, KB-Fe, and BB-Fe samples. The marked decrease in the intensity of the Al–OH band near 910 cm^{-1} suggests the partial dissolution of aluminosilicate phases and the removal of aluminum during acid activation [12]. Conversely, the persistence of the Si–O stretching bands around 1025 cm^{-1} indicates the greater resistance of silica-rich phases to acid attack [12]. The appearance or enhancement of absorption bands within the 600–700 cm^{-1} region may be attributed to Fe–O and/or Fe–OH vibrational modes associated with iron oxyhydroxide species deposited on the clay surface [44]. Furthermore, the presence of a broad, low-intensity band around 3400 cm^{-1} suggests the occurrence of hydroxyl groups and adsorbed water molecules associated with the ferrihydrite-modified materials [45]. Overall, the FTIR results corroborate the mineralogical transformations induced by calcination and highlight the chemical modifications resulting from acid activation and ferrihydrite deposition.

3.6. Morphological and Microstructural Analysis

Morphological observations revealed clear differences between the raw clays (KR, KB, and BB) and the samples subjected to acid activation followed by ferrihydrite deposition (KR-Fe, KB-Fe, and BB-Fe) (Figure 6, Figure 7, and Figure 8). The raw clays exhibited relatively compact lamellar structures composed of stacked plate-like particles, with surfaces partially covered by mineral phases rich in iron and aluminum. Similar morphologies have been widely reported for unmodified natural clays [31,46]. Following calcination at 750°C, a progressive disruption of the lamellar organization was observed, reflecting the structural modifications induced by the dehydroxylation of phyllosilicates, particularly kaolinite, and the subsequent formation of amorphous metakaolinite [29]. Acid activation with hydrochloric acid further altered the morphology of the materials through the partial dissolution of alumina-rich phases and other acid-soluble constituents, thereby generating a more irregular and porous structure [47,48]. Subsequent ferrihydrite deposition resulted in noticeable changes in surface morphology. The modified samples displayed rougher and more heterogeneous surfaces, characterized by the presence of fine particulate aggregates distributed over the clay matrix. These morphological features may be associated with the incorporation of iron-bearing phases onto the surface of the acid-treated clays [49,50]. In addition, EDX analyses revealed an increase in iron content in the modified samples compared with the corresponding raw materials, providing further evidence of the successful modification of the clay matrix. Overall, the sequence of thermal treatment, acid activation, and ferrihydrite deposition induced substantial structural and compositional changes in the investigated materials. These modifications are expected to influence the physicochemical and surface properties of the clays and

may contribute to their suitability for future environmental applications. Nevertheless, the implications of these modifications for adsorption processes remain to be validated through dedicated adsorption studies involving representative contaminants and appropriate performance assessments.

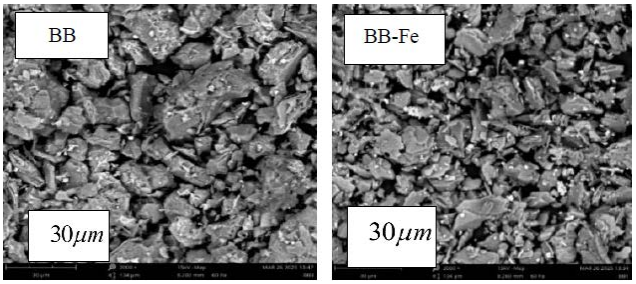

Figure 6. Morphology of BB and BB-Fe samples

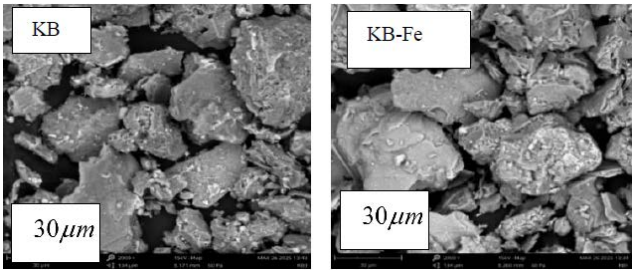

Figure 7. Morphology of KB and KB-Fe samples

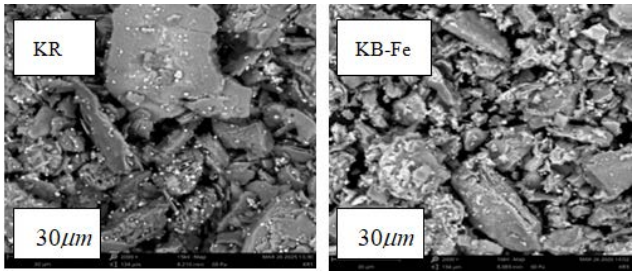

Figure 8. Morphology of KR and KR-Fe samples

The results of the EDS elemental analysis presented in Table 4 indicate that the raw clay samples are mainly composed of silicon (Si), aluminum (Al), and iron (Fe), together with smaller amounts of K, Mg, Ca, Na, and Ti. The aluminum content ranges from 18.81 wt.% in KB to 22.86 wt.% in KR. The predominance of Si and Al is consistent with the X-ray fluorescence (XRF) results, which identified SiO_2 and Al_2O_3 as the major oxide constituents of the investigated materials. Iron is particularly abundant in the KR sample (30.06 wt.%), suggesting a greater contribution of iron-bearing mineral phases. This observation is in agreement with the XRD results, which revealed the presence of goethite in the raw clays [53]. The variations in elemental composition among the samples reflect differences in their mineralogical composition and geological origin.

The treatment of calcined clays (KR-Fe, KB-Fe, and BB-Fe) with 5 $mol \cdot L^{-1}$ HCl, followed by ferrihydrite deposition, induced noticeable changes in their elemental composition. A decrease in Al and Mg contents was observed in the modified samples, suggesting the partial dissolution of alumina- and magnesium-bearing phases during acid activation [12]. Concurrently, an increase in Fe content was detected, which may be attributed to the incorporation of iron-bearing phases resulting from the ferrihydrite deposition process [11]. This enrichment in iron is consistent with the modification procedure employed and supports the successful alteration of the clay matrix. Furthermore, the detection of Cl and S in the KR-Fe, KB-Fe, and BB-Fe samples may be associated with residual chloride ions originating from the hydrochloric acid treatment and sulfate species related to the ferrihydrite deposition step. Despite repeated washing, trace amounts of these elements may remain adsorbed on the surface of the modified materials.

Table 4. EDS analysis by mass composition of the clays

Samples	KR	KB	BB	KR-Fe	KB-Fe	BB-Fe
Si	40.73	46.56	55.66	39.53	41.49	49.91
Al	22.86	18.81	21.14	13.84	10.23	12.39
Fe	30.06	22.90	16.80	35.16	35.95	30.98
K	2.82	4.55	5.64	1.64	2.36	3.52
Ti	1.77	1.33	0.63	1.64	1.04	
Ca		2.31	0.12		1.51	
Mg	1.21	2.26		0.17	0.41	0.12
Na	0.14	1.28			2.97	
Mn	0.41			0.23		0.56
S				3.80	2.54	2.32
Cl				4.00	1.5	0.19

3.7. Adsorbent Properties

Table 5 and Figure 9 and Figure 10 summarize the textural and surface properties of the raw clays (KR, KB, and BB), the clays calcined at 750°C (KR-Cal, KB-Cal, and BB-Cal), and the clays subjected to acid activation followed by ferrihydrite deposition (KR-Fe, KB-Fe, and BB-Fe). The results reveal noticeable variations in the iodine number (IIN), methylene blue index (MBI), BET specific surface area (S_BET), and point of zero charge (pH_PZC), reflecting the modifications induced by the different treatments. Iodine Number and Methylene Blue Index The iodine number, commonly used as an indicator of the accessibility of microporous domains and the presence of site capable of interacting with small molecules, is presented in Table 5. For the raw samples, iodine numbers ranged from 505 to 593 $mg \cdot g^{-1}$, with the highest value recorded for KR. Calcination at 750°C resulted in a slight increase in iodine number for BB and KB, whereas a more pronounced increase was observed for KR. These changes may be associated with the structural transformations induced by thermal treatment, particularly the dehydroxylation of kaolinite and the formation of metakaolinite. Ferrihydrite deposition led to a further increase in iodine number, especially in the KR-Fe sample. This trend suggests that the successive treatments modified the textural characteristics of the materials, possibly through the generation of additional accessible surface domains and changes in pore organization. However, iodine number values should be interpreted cautiously, as they do not directly reflect adsorption performance in the absence of specific adsorption experiments. The methylene blue index (MBI), which provides information related to the accessibility of larger molecules to the external surface and mesoporous domains of the materials, remained relatively constant at

approximately 330 mg·g⁻¹ for all samples. This limited variation suggests that the treatments had only a minor effect on the mesoporous characteristics and external surface accessibility of the investigated clays, regardless of their geographical origin [41].

Table 5. Chemical Characteristics

Samples	I_{Io} (mg/g)	I_M (mg/g)	S_{BET}(m^2/g)	pH_{pcn}
KR	593.55 ± 0.2	320.21 ± 0.065	49.98	6.1 ± 0.1
KR-Cal	699.86 ± 0.2	329.88 ± 0.065	57.71	7.1 ± 0.1
KR-Fe	1373.14 ± 0.2	329.88 ± 0.065	75.8	5.8 ± 0.1
KB	511.50 ± 0.15	329.54 ± 0.005	52.33	5.3 ± 0.2
KB-Cal	524.45 ± 0.15	330 ± 0.005	62.93	5.9 ± 0.2
KB-Fe	735.29 ± 0.15	330.3 ± 0.0050	87.32	4.8 ± 0.2
BB	505.03 ± 0.1	329.99 ± 0.025	37.72	5.4 ± 0.2
BB-Cal	517.97 ± 0.1	330.02 ± 0.025	41.93	6.3 ± 0.2
BB-Fe	524.45 ± 0.1	329.28 ± 0.025	65.26	5 ± 02

Textural properties (Specific surface area and N_2 adsorption isotherms) For all samples, the BET plots exhibited satisfactory linearity within the relative pressure range of $0.05 < P/P_0 < 0.35$, confirming the appropriateness of the selected pressure interval and the reliability of the calculated specific surface areas [55,56] (Figure 9). The measured BET specific surface areas essentially correspond to the external surfaces accessible to nitrogen molecules. As summarized in Table 5, the specific surface areas ranged from 37.72 to 52.33 m²·g⁻¹ for the raw clays, from 41.93 to 62.93 m²·g⁻¹ for the calcined clays, and from 65.26 to 87.32 m²·g⁻¹ for the ferrihydrite-modified clays. The evolution of the BET specific surface area followed the same trend as that observed for the iodine number, suggesting that the successive treatments induced modifications in the textural characteristics of the materials [41]. The increase in specific surface area observed after calcination and ferrihydrite deposition may be attributed to the structural transformations induced by thermal treatment, including the dehydroxylation of phyllosilicates, as well as to the morphological changes associated with acid activation and ferrihydrite incorporation. Similar trends have been reported for modified clay materials in previous studies [57,58,59]. The specific surface areas of the BB and KR samples are comparable to those reported for natural kaolinitic clays [60,61]. Although these two samples exhibit similar mineralogical compositions, the KR sample, characterized by a higher iron content, displayed a greater specific surface area than BB. This observation suggests that iron-bearing phases may influence the development of surface characteristics [59,62]. The highest BET surface areas were obtained for the KB series, which may be related to the presence of smectitic phases in combination with other associated minerals [57,61]. Although these values remain lower than those commonly reported for pure montmorillonite, they indicate that the Katiola clay is composed of a heterogeneous assemblage of kaolinite, montmorillonite, and illite, with additional contributions from secondary mineral phases derived from the alteration of the parent material [55,63]. Comparison with recent literature shows that the BET surface areas obtained in this study are generally within, or slightly above, the range reported for several natural and modified clay materials [64,65,66,67,68,69]. Kaolinite-rich clays typically exhibit specific surface areas ranging from 15 to 45 m²·g⁻¹, whereas thermally treated materials may develop larger surface areas as a result of dehydroxylation and structural reorganization [64]. Similarly, clay materials modified through chemical treatments or iron oxyhydroxide deposition often display BET surface areas ranging from 60 to 85 m²·g⁻¹ [65,66,67,68]. In this context, the maximum value obtained for the KB-Fe sample (87.32 m²·g⁻¹) lies within the upper range reported for modified clay materials in recent studies. Overall, the results demonstrate that the combination of calcination, acid activation, and ferrihydrite deposition significantly altered the textural properties of the investigated clays, leading to an increase in the specific surface area accessible to nitrogen molecules. These observations are consistent with the findings of Blattmann and Plötze [55] and other studies dealing with the modification of clay materials [65,66,67,68,69]. The enhanced textural characteristics observed in the modified samples highlight the effectiveness of the treatment strategy employed in tailoring the surface properties of the Ivorian clays.

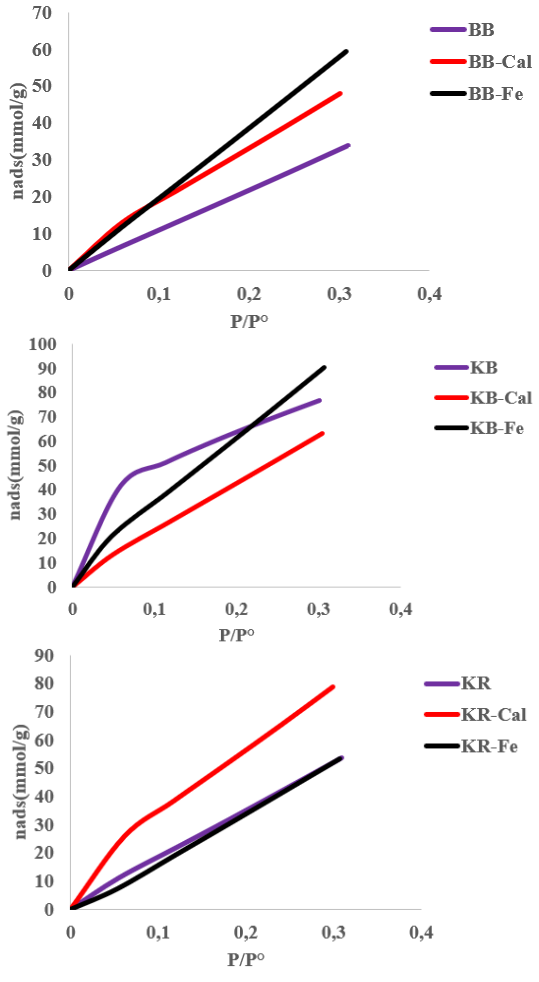

Figure 9. Nitrogen adsorption isotherms at 77 K on the samples

Point of Zero Charge (pH_pzc) The point of zero charge (pH_pzc) values of the investigated samples ranged from 4.8 (KB-Fe) to 7.1 (KR-Cal) (Table 5 and Figure 10). The pH_pzc corresponds to the pH at which the net surface charge of the material is zero and is therefore an important parameter governing the acid–base behavior of solid surfaces in aqueous media. At pH values above the pH_pzc, the surface tends to acquire a negative charge, whereas at pH values below the pH_pzc, it becomes positively charged [41,42]. The results indicate that acid activation followed by ferrihydrite deposition generally led to a decrease in the pH_pzc values of the modified clays. This trend may be related to the partial dissolution of alumina-rich phases during acid treatment, resulting in a relative enrichment of silica at the material surface. According to Dehou et al. [12], acid activation can induce significant dealumination of clay minerals, thereby modifying their surface chemical characteristics. This interpretation is supported by the findings of Tschapek et al. [71], who demonstrated that the pH_pzc of Al_2O_3–SiO_2 systems increases with increasing Al_2O_3 content. Consequently, a reduction in alumina content relative to silica may lead to lower pH_pzc values, reflecting changes in the surface acid–base properties of the materials [71]. The observed shifts in pH_pzc therefore provide evidence that the successive treatments applied in this study altered the surface characteristics of the Ivorian clays.

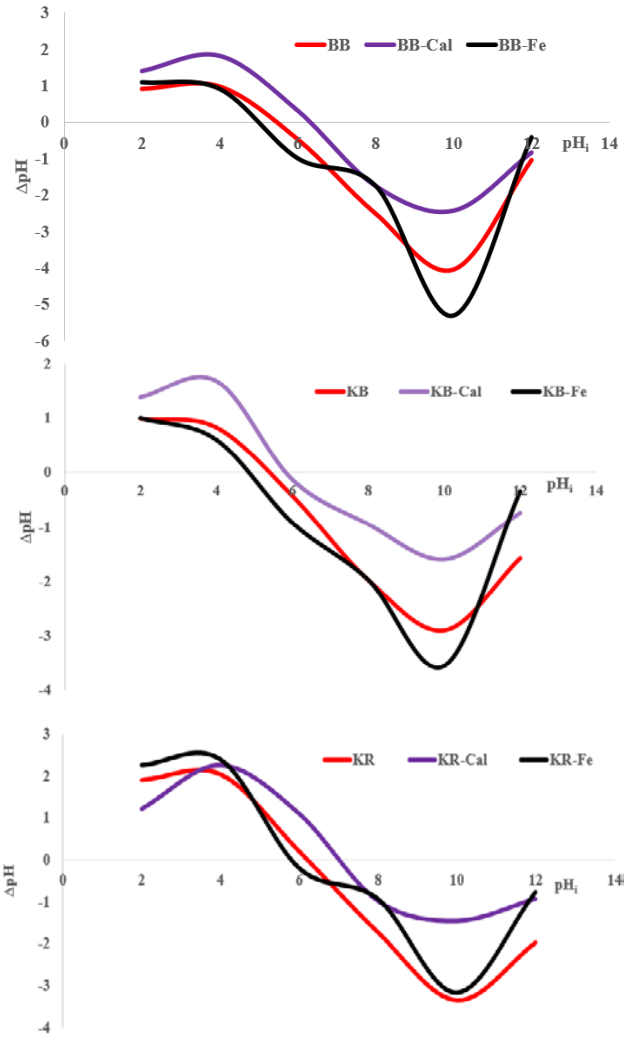

Figure 10. Effect of pH variation in aqueous solution on clays

4. Conclusion

This study aimed to characterize natural Ivorian clays subjected to thermal treatment and subsequent modification by iron oxyhydroxide (FeOOH) deposition, in order to assess the effects of these treatments on their physicochemical, mineralogical, morphological, and textural properties. The results demonstrated that calcination at 750°C induced the dehydroxylation of phyllosilicates and the transformation of kaolinite into amorphous metakaolinite, leading to significant structural modifications. Acid activation promoted the partial dissolution of alumina-rich phases, resulting in changes in surface chemistry and an increase in the accessibility of the porous structure. Ferrihydrite deposition further altered the composition and morphology of the clays, as evidenced by the increase in iron content and the development of rougher and more heterogeneous surfaces. The combined treatments also induced substantial changes in the textural characteristics of the materials. In particular, the ferrihydrite-modified clays exhibited higher BET specific surface areas and iodine numbers than the corresponding raw materials, indicating the effectiveness of the modification strategy in tailoring the surface properties of the investigated clays. The shifts observed in the point of zero charge (pH_pzc) further confirmed the alteration of the acid–base characteristics of the clay surfaces following treatment. Overall, the findings highlight the potential of thermal treatment, acid activation, and ferrihydrite deposition as effective approaches for modifying the physicochemical and textural properties of Ivorian clays. These results contribute to a better understanding of the transformations induced by these treatments and provide a scientific basis for future investigations into the application of such modified materials in environmental remediation processes. Furthermore, they emphasize the value of locally available clay resources as low-cost materials that can be engineered for potential use in sustainable water treatment technologies.

Conflicts of Interest

The authors declare no conflicts of interest regarding this article.

References

[1] Itodo, A. U., Abdulrahman, F.W., Hassan, L. G., Maigandi, S. A. and Itodo, H. U. Application of Methylene Blue and Iodine Adsorption in the Measurement of Specific Surface Area by four Acid and Salt Treated Activated Carbons. *New York Science Journal*, (5), p. 3, fevrier 2010.

[2] Sharma, G., Sharma, S. and Stadler, F. J. Activated Carbon as Superadsorbent and Sustainable Material for Diverse Applications. *Adsorption Science and Technology*, (2022), p. 4184809, janvier. 2022.

[3] Méité, N., Kouakou, L., Kouamé, A, Pohan, A., Sanou, I., Cissé, G., Kouakou, C. and Andji-Yapi, Y. Study of the Influence of Clay in the Degradation of Methylene Blue by Photo-Fenton Process. *Materials Sciences and Applications*, (15), p. 538-557, Avril 2024.

[4] degoke, K.A., Adesina, O.O., Okon-Akan, O.A., Adegoke, O.R.,

Olabintan, A.B. and Ajala, O.A. Sawdust-biomass based materials for sequestration of organic and inorganic pollutants and potential for engineering applications. *Current Research in Green and Sustainable Chemistry*, (5), p. 100274, Janvier 2022.

[5] Kouakou, L.P.M., Karidioula, D., Manouan, M.R.W., Pohan, A.G.L., Cissé, G. and Konan, L.K. Use of two clays from Côte d'Ivoire for the adsorption of methyl red from aqueous medium. *Chemical Physics Letters*., (810), p. 140183, janier. 2023.

[6] Sanou, I., Bamogo, H., Sanou, A., Ouedraogo, M., Saadi, L., Waqif, M. and Millogo, Y.Adsorption of Methylene Blue in Aqueous Medium by Activated Carbon from Peanut Shells. *Chemistry Africa*., (7), p. 2777-2794, juillet 2024.

[7] Amadou Kiari, M. N., Ouattara, L. Y. Adamou Ibro, A., Ibrahim Grema, M. H., Sanou, A., Traore, A., Malam Alma M. M. and Yao, K. B. Optimization by Response Surface Methodology of Methylene Blue Removal in Aqueous Solution on Bioadsorbent Based on Hyphaene Thebaica Shells. *International Journal of Engineering Research in Africa*, (78), p. 1-20, février 2026.

[8] Moses, K. L., Pascal, B., Alfred, K. N., Marie, L., Joseph, S., Hervé, M. and Florence P. Sodium-Treated Iron-Bridged Clay for Arsenic Removal in the Presence of Lead and Cadmium: A Comparative Study. *Journal of Global Ecology and Environment*., (21), no 4, p. 139-150, novembre 2025.

[9] Gorączko, A. and Topoliński, S. Particle Size Distribution of Natural Clayey Soils: A Discussion on the Use of Laser Diffraction Analysis (LDA). *Geosciences*, (10), p. 55, janvier 2020.

[10] Leiva, W. H., Toro, N. Robles, P., Quezada, G. R., Salazar, I. and Jeldres, R. Clay Tailings Flocculated in Seawater and Industrial Water: Analysis of Aggregates, Sedimentation, and Supernatant Quality. *Polymers*, (16), p. 1441, mai 2024.

[11] Allahdin, O. Elimination (par adsorption sur la brique activée) de polluants métalliques dans les eaux de la République Centrafricaine et les pays en voie de développement. Aspects texturaux, physico-chimiques (électro) cinétiques et thermodynamiques. These de Doctorat, Université Lille 1, 2014.

[12] Dehou, S.-C. Etude des propriétés d'adsorption des oxyhydroxydes de fer déposé sur un support naturel (la brique) : application à l'élimination du fer dans les eaux de forages en République Centrafricaine. These de Doctorat, Université Lille 1 Science et Technologies., 2011.

[13] Sanou, Y. and Paré, S. Etude du pouvoir adsorbant d'une latérite dopée par la ferrihydrite pour l'élimination de l'arsenic (V) des eaux. *Journal de la Société Ouest-Africaine de Chimie*, (050), p. 41-49, 2021.

[14] N'Cho, W. C. Contrôle de la porosité en voie acide ou basique et de l'hydrophobie du matériau géopolymère. These de Doctorat, Université de Limoges, P. 169, 2024.

[15] Lenoble, V. Elimination de l'Arsenic pour la production d'eau potable: oxydation chimique et adsorption sur des substrats solides innovants. These de Doctorat, Université de Limoges, 2003.

[16] Yvon, J., Lietard, O., Cases, J.-M. and Delon, J.-F. Minéralogie des argiles kaoliniques des Charentes. Bulletin de Minéralogie, p. 431-437, 1982.

[17] Babakoua, D. D., Fiaty, K., Charcosset, C., Tchegueni, S., Anove, K., Koriko, M. and Tchangbedji G. Characterization and Pozzolanic Reactivity of Two Togolese Clays for Use as Supplementary Cementitious. *Journal of Materials Science and Chemical Engineering*, (13), p. 31-54, 2025.

[18] Djonga, W. G., Noubissié, E. and Noumi, G. B. Discoloration test of a slaughterhouse effluent by adsorption on two adsorbents produced from sawdust of Khaya senegalensis and Pinus sp. *Results in Engineering*, (4), p. 100068, décembre 2019.

[19] Nshimiyimana, P., Fagel, N., Messan, A., Wetshondo, D.O. and Courard, L. Physico-chemical and mineralogical characterization of clay materials suitable for production of stabilized compressed earth blocks. Construction and Building Materials, (241), p. 118097, avril 2020.

[20] Atsé, W. A., Essi, M. M.-M. M., Doubi, B. I. H. G., Kamagaté, M., Aké, A. P. and Kouamé, A. N. Physico-Chemical Characterization of Two Dabou Clays with a View to Use Them in the Treatment of Dyeing Wastewater. *Journal of Minerals and Materials Characterization and Engineering*, (10), p. 505-517, 2022.

[21] Bakary Soro, S., Coulibaly, M., Paul Gauly, L., N'Dri, S.R., Sanou, A. and Trokourey, A. Characterization of Clay Materials from Côte d'Ivoire: Possible Application for the Electrochemical Analysis. *Journal of Materials Science Research*, (12), p. 51, mai 2023.

[22] Gauly, L.P., Coulibaly, M., Soro, S.B., Kouadio, K.S., N'Dri, S.R. and Sanou, A. Characterization and enhanced performance of Ivorian clays as potential modifiers in carbon paste electrodes. *Discover Applied Sciences*, (7), p. 128, février 2025.

[23] Daou, I., Lecomte-Nana, G., Tessier-Doyen, N., Peyratout, C., Gonon, M. and Guinebretiere, R. Probing the Dehydroxylation of Kaolinite and Halloysite by In Situ High Temperature X-ray *Diffraction. Minerals*, (10), p. 480, mai 2020.

[24] Daou, I., Mocuta, C., Lecomte-Nana, G. L., Tessier-Doyen, N., Peyratout, C., Guinebretière, R. and Thiaudière, D. Dehydroxylation of Kaolinite and Halloysite-Rich Samples: An In Situ Study of the Texture and Structural Evolutions. *Minerals*, (13), p. 1418, novembre 2023.

[25] Sanou, A., Coulibaly, M., N'dri, S.R., Tămaș, T.L., Bizo, L., Frentiu, T., Covaci, E., Abro, K. D. M., Dablé, P. J-M. R., Yao, K. B., Fort, C. I. and Turdean, G. L. Raw clay material-based modified carbon paste electrodes for sensitive heavy metal detection in drinking water. *Journal of Materials Science*, (59), p. 13961-13977, août 2024.

[26] Niamien Kouamé, A., Koffi Konan, L. and Irié Hervé Gouré Doubi, B. Microstructure and Mineralogy of Compressed Earth Bricks Incorporating Shea Butter Wastes Stabilized with Cement. *Advances in Materials*, (10), p. 67, 2021.

[27] Fort, C.I., Sanou, A., Coulibaly, M., Yao, K.B. and Turdean, G.L. Green modified electrode for sensitive simultaneous heavy metal ions electrodetection. *Sensors and Actuators B: Chemical*, (418), p. 136326, novembre 2024.

[28] Tejeogue, J. P. N., Djakba, R., Fotsop, C. G., Dobe, N., Mouhamadou, S., Wangmene, B. and Harouna, M. Systematic metronidazole adsorption performance onto montmorillonite clay: Parametric study, process modelling and RSM optimization. Results in Chemistry, (14), p. 102153, mars 2025.

[29] Konan, K. L., Peyratout, C., Smith, A., Bonnet, J.-P., Rossignol, S. and Oyetola, S. Comparison of surface properties between kaolin and metakaolin in concentrated lime solutions. *Journal of colloid and interface science*, (339), p. 103-109, novembre 2009.

[30] Madejová, J. and Komadel, P. Baseline studies of the clay minerals society source clays: infrared methods. *Clays and clay minerals*, (5), p. 410-432, Octobre 2001.

[31] Murray, H. H. Applied Clay Mineralogy. Elsevier. 2007, 179 p.

[32] Konan, K. L., Soro J., Andji J.Y.Y., Oyetola S. and Kra G. Etude comparative de la déshydroxylation/amorphisation dans deux kaolins de cristallinité différente. *Journal de la Société Ouest-Africaine de Chimie*, (030), p. 29-39, août, 2010.

[33] Deer, W. A., Howie, R. A. and Zussman, J. An Introduction to the Rock-Forming Minerals. *Mineralogical Society of Great Britain and Ireland*, 2013.

[34] Sabir, B. B., Wild, S. and Bai, J. Metakaolin and calcined clays as pozzolans for concrete: a review. Cement Concrete Composite, (23), p. 441-454, décembre 2001.

[35] Tra, B. G. A., Bamba, D., Méité, N., Kouamé, A. N., Coulibaly, M. and Konan, K. L. Physico-Chemical, Mineralogical, and Morphological Characterizations of Three Clays from Côte d'Ivoire with a View to Their Use in Adsorption. *Journal of Materials Science and Chemical Engineering*, (14), p. 31-52, Avril 2026.

[36] Ladjal, N., Terchi, S. and Debih, H. High efficiency adsorption performance of basic dye (crystal violet) onto algerian montmorillonite. *Studii şi Cercetări Ştiinţifice*, p. 001-018, Octobre 2024.

[37] Marco-Brown, J.L., Guz, L., Olivelli, M.S., Schampera, B., Torres Sánchez, R.M. and Curutchet, G. New insights on crystal violet dye adsorption on montmorillonite: Kinetics and surface complexes studie. *Chemical Engineering Journal*, (333), p. 495-504, février 2018.

[38] Ake, A.P., Coulibaly, V., Ouattara, Y.N., Kouadio, L.M., Kouakou, L.P.M. and Aketchi, T.L. Study of the Influence of Some Ions on the Adsorption of Phosphates by Clay Materials from Côte d'Ivoire. *International Research Journal of Pure and Applied Chemistry*, (26), p. 96-111, mars 2025.

[39] Drits, V.A., Zviagina, B.B., Sakharov, B.A., Dorzhieva, O.V. and Savichev, A.T. New Insight into the Relationships Between Structural and Ftir Spectroscopic Features of Kaolinites. Clays and Clay Mineral, (69), p. 366-388, juin 2021.

[40] Aké, A.P., Coulibaly, V., Kouamé, N., Kedi, A.B., Sei, J. and Oyetola, S. Study of the status of iron in clay materials from Côte d'Ivoire for their use as phosphate adsorbents », *RAMRES*

Sciences des Structures et de la Matière, (6), 63-90, 2022.

[41] Nwosu, F.O., Ajala, O.J., Owoyemi, R.M. and Raheem, B.G. Preparation and characterization of adsorbents derived from bentonite and kaolin clays. *Applied Water Science*, (8), 195, Octobre 2018.

[42] Massesse-Loudi, M., Boukongou, A., Mongo, D. and Barhé, T. Study of the Adsorption of Difenoconazole on Char in Aqueous Medium. *American Journal of Chemical Engineering*, (13), p. 14-19, février 2025.

[43] Sanou, I., Zoungrana, S., Ouedraogo, M., Sanou, A. and Millogo, Y. Evaluation of the Pozzolanic Activity of Metakaolin, Glass Powder and Silica Powder for Use in Cementitious Mortars. *Studia Universitatis Babeş-Bolyai Chemia*., p. 49-66, décembre 2024.

[44] Rezig, w., Elaziouti, A., Laouedj, N. and M. Hadjel, M. Synthesis and characterization of novel calcined ferrihydrite-modified diatomite (FMD3X6) and its UVA light-assisted heterogeneous photodegradation of VG3 dye. *Desalination Water Treatment*, (271), p. 254-271, septembre 2022.

[45] Tian, X., Xie, Q., Chai, G. and Li, G. Simultaneous adsorption of As(III) and Cd(II) by ferrihydrite-modified biochar in aqueous solution and their mutual effects. *Scientific Reports*, (12), p. 5918, avril 2022.

[46] Bergaya, F. and Lagaly, G. Chapter 1 General Introduction: Clays, Clay Minerals, and Clay Science. *Developments in Clay Science*, (1), p. 1-18, 2006.

[47] Komadel, P., Schmidt, D., Madejová, J. and Ćíčel, B. Alteration of smectites by treatments with hydrochloric acid and sodium carbonate solutions. *Applied clay science*, (5), p. 113-122, août 1990.

[48] Bendou, S. and Amrani, M. Effect of Hydrochloric Acid on the Structural of Sodic-Bentonite Clay. *Journal of Minerals and Materials Characterization and Engineering*, (02), p. 404-413, 2014.

[49] Cornell, R. M. and Schwertmann, U. The Iron Oxides: Structure, Properties, Reactions, Occurences and Uses, *1re édition Wiley*, 2003.

[50] Botto, I. L., Tuti, S., Gonzalez, M. J. and Gazzoli, D. Correlation between Iron Reducibility in Natural and Iron-Modified Clays and Its Adsorptive Capability for Arsenic Removal. *Advances in Materials Physics and Chemistry*, (06), p. 129-139, Mai 2016.

[51] Liu, R. and Zhao, D. Reducing leachability and bioaccessibility of lead in soils using a new class of stabilized iron phosphate nanoparticles. *Water Research*, (41), p. 2491-2502, juin 2007.

[52] Chen, L., Xin, H., Fang, Y., Zhang, C., Zhang, F., Cao, X., Zhang, C. and Li, X. Application of Metal Oxide Heterostructures in Arsenic Removal from Contaminated Water. *Journal of Nanomaterials*, (2014) p.10, janvier 2014.

[53] Taïpabé, D., Doko, K. V., Datchossa, T. A., Abdourahamane, A. I., Mandela, T., Sanou, A. and Gibigaye, M. Characterization of a lateritic soil in Chad with a view to its use in ecoconstruction ; *Journal of Materials and Environmental Science*, (16), p. 1189-1209, Juin 2025.

[54] Mahamane, N.A.K, Fanou, G.D., Konan, A.T.S., Ouattara, A., Kone, H., Malam, A.M.M., Assidjo, E.N. and Yao, K.B. Process conditions optimization of plant waste-derived microporous activated carbon using a full factorial design and genetic algorithm. *Journal of Materials and Environmental Science*, p. 884-899, août 2022.

[55] Blattmann, T. M. and Plötze, M. BET-based mineral surface area quantification comparing nitrogen with water. *Applied Clay Science*, (258), p. 107477, septembre 2024.

[56] Sing, K. S. W., Everett, D. H., W. Haul, R. A., Moscou, L., Pierotti, R. A., Rouquerol, J. and Siemieniewska, T. eporting physisorption data for gas/solid systems with special reference to the determination of surface area and porosity. *International Union of Pure and Applied Chemistry*, (57), p. 603-619, 1985.

[57] Bhattacharyya, K. Kaolinite and montmorillonite as adsorbents for Fe(III), Co(II) and Ni(II) in aqueous medium. *Applied Clay Science*, (41), p. 1-9, septembre 2008.

[58] Hiemstra, T., Mendez, J. C. and Li, J. Evolution of the reactive surface area of ferrihydrite: time, pH, and temperature dependency of growth by Ostwald ripening. *Environmental Science Nano*, (6), p. 820-833, Janvier 2019.

[59] Mendez, J. C. and Hiemstra, T. Surface area of ferrihydrite consistently related to primary surface charge, ion pair formation, and specific ion adsorption. *Chemical Geology*, (532), p. 119304, janvier 2020.

[60] Bhattacharyya, K. G. and Gupta, S. S. Adsorption of a few heavy metals on natural and modified kaolinite and montmorillonite: A review. *Advances in colloid and interface science*, (140), p. 114-131, août 2008.

[61] Sen Gupta, S. and Bhattacharyya, K. G. Adsorption of heavy metals on kaolinite and montmorillonite: a review. *Physical Chemistry Chemical Physics*, (14), p. 6698, Mars 2012.

[62] Sei, J., Jumas, J. C., Olivier-Fourcade, J., Quiquampoix, H. andStaunton, S. Role of Iron Oxides in the Phosphate Adsorption Properties of Kaolinites from the Ivory Coast. *Clays and Clay minerals*, (50), p. 217-222, avril. 2002.

[63] Demirbas, A. Agriculturally based activated carbons for the removal of dyes from aqueous solutions: A review. *Journal of Hazardous Materials*, (167) p. 1-9, août 2009.

[64] Alomari A. D. A. Chemically modified clay for adsorption of contaminants: trends, advantages and limitations - a concise review. *International Journal of Environmental Analytical Chemistry*, (105), p. 2302-2325, août, 2025.

[65] Li Y., Yuan X., Guan X., Bai J., and Wang H. One-pot synthesis of siliceous ferrihydrite − coated halloysite nanorods in alkaline medium: Structure, properties and cadmium adsorption performance. *Journal of Colloid and Interface Science*, (636), p. 435-449, avril, 2023.

[66] Wang P., Shen X., Qiu S., Zhang L., Ma Y. and Liang J. Clay-Based Materials for Heavy Metals Adsorption: Mechanisms, Advancements, and Future Prospects in Environmental Remediation. *Crystals*, (14), p. 1046, novembre, 2024.

[67] Perez-Lapid N., Cohen K., Manor N. K. and Radian A. Montmorillonite decorated with amorphous iron-(hydr)oxides nanoparticles for effective phosphate removal and recovery from wastewater. *Applied Clay Science*, (257), p. 107448, septembre, 2024.

[68] Yang X., Zhou Y., Hu J., Zheng Q., Zhao Y., Lv G. and Liao L. Clay minerals and clay-based materials for heavy metals pollution control. *Science of the Total Environment*, (954), p. 176193, décembre, 2024.

[69] Xie S., Huang L., Su C., Yan J., Chen Z., Li M., Du M and Zhang H. Application of clay minerals as adsorbents for removing heavy metals from the environment. Green and Smart Mining Engineering, (1), p. 249-261, septembre, 2024.

[70] Wu, K., Li, Y., Liu, T., Huang, Q., Yang, S. Wang, W. and Jin, P. The simultaneous adsorption of nitrate and phosphate by an organic-modified aluminum-manganese bimetal oxide: Adsorption properties and mechanisms. *Applied Surface Science*, (478), p. 539-551, juin 2019.

[71] Tschapek M., Tcheichvili L. and Wasowski C. The point of zero charge (pzc) of kaolinite and SiO_2 +AI_2 O_3 mixtures Clay. Miner., (10), p. 219-229, décembre, 1974.